THE JOURNAL OF PHYSICAL CHEMISTRY LETTERS
A JOURNAL OF THE AMERICAN CHEMICAL SOCIETY

pubs.acs.org/JPCL

Letter

Revealing Elusive Intermediates of Platinum Cathodic Corrosion through DFT Simulations

Iman Evazzade, Alexandra Zagalskaya, and Vitaly Alexandrov*

Cite This: *J. Phys. Chem. Lett.* 2022, 13, 3047−3052

Read Online

ACCESS | Metrics & More | Article Recommendations | Supporting Information

ABSTRACT: Cathodic corrosion of metals discovered more than 120 years ago remains a poorly understood electrochemical process. It is believed that the corrosion intermediates formed during cathodic polarization are extremely short-lived species because of their high reactivity. Together with the concurrent vigorous hydrogen evolution, this makes it challenging to investigate the reaction mechanism and detect the intermediates experimentally. From a computational standpoint, the process also presents a serious challenge as it occurs at rather low negative potentials in concentrated alkaline solutions. Here, we use density-functional-theory calculations to elucidate the identity of reaction intermediates and their reactivity at the Pt(111)/electrolyte interface. By controlling the electrode potential in an experimentally relevant region through constant Fermi-level molecular dynamics, we reveal the formation of alkali cation-stabilized Pt hydrides as intermediates of cathodic corrosion. The results also suggest that the found Pt anions could discharge at the interface to produce H_2 by reacting with either surface-bound hydrogen species or solution water molecules.

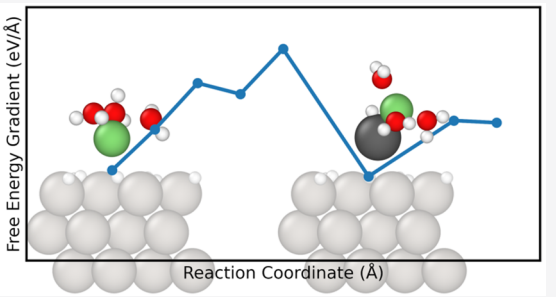

The phenomenon of metal corrosion appears to be as old as electrochemistry itself.[1−5] Corrosion of metal surfaces is most commonly associated with an anodic process. During anodic corrosion a metal is oxidized at positive potentials triggering materials dissolution in the form of metal cations. Such anodic corrosion of metallic systems has previously been the primary focus of both experimental and theoretical investigations.[6−16] In contrast, cathodic corrosion is a far less understood electrochemical process. One reason for the limited attention to this phenomenon in the past is the discovery of cathodic protection first described by Davy back in 1824.[3] It has been implicated that cathodically protected metals become immune to corrosion. If this were true, then the most reduced form of metal ions would be neutral species. Although presently available Pourbaix diagrams for metals in aqueous media indeed contain neutral metals as the most reduced species, it is known that metals can be stabilized as anions such as in Zintl phases.[17−21] It has been thus proposed in the literature that analogous metal anions of yet unknown composition could be formed at the electrochemical interface during cathodic corrosion.[22−24] The cathodically generated corrosion intermediates were hypothesized to be rapidly consumed by reacting with water. This process leads to the recovery of the original neutral metal that precipitates at the surface, changing its morphology.[25] However, such corrosion intermediates have never been detected directly in experiments, which is presumably due to their short lifetime at the interface.

It is established that cathodic corrosion of metals can occur under both mild conditions (pH 7 and −1 V vs NHE) and very harsh conditions (e.g., 10 M NaOH electrolyte and −10 V vs NHE). For example, dissolution of Pt was observed even at moderately negative potentials during the oxygen reduction reaction (ORR) in water.[26−28] In concentrated electrolytes such as 10 M NaOH, cathodic corrosion of Pt was observed to commence already at −0.4 V vs RHE, while in 1 M NaOH, the corrosion onset potential was measured at −0.6 V vs RHE.[24,29] It is also known that cathodic corrosion is both electrode- and electrolyte-specific. In experiments, the presence of alkali cations from the electrolyte was revealed to be critical for promoting cathodic corrosion. It was demonstrated on the examples of Pt, Au, and Rh that metal corrosion becomes more pronounced when going from LiOH to NaOH and KOH solution.[30] However, it remains unknown how the atomic-scale mechanism and kinetics of cathodic corrosion vary across different electrode materials, electrolytes, and reaction conditions.

Despite a common perception of metal corrosion as a detrimental process, it can also be utilized in favorable ways. Specifically, cathodic corrosion has been shown to be a promising approach to rapidly synthesize metal and metal-oxide nanoparticles with homogeneous shape and size without

Received: December 26, 2021
Accepted: March 28, 2022
Published: March 30, 2022

https://doi.org/10.1021/acs.jpclett.1c04187
J. Phys. Chem. Lett. 2022, 13, 3047−3052

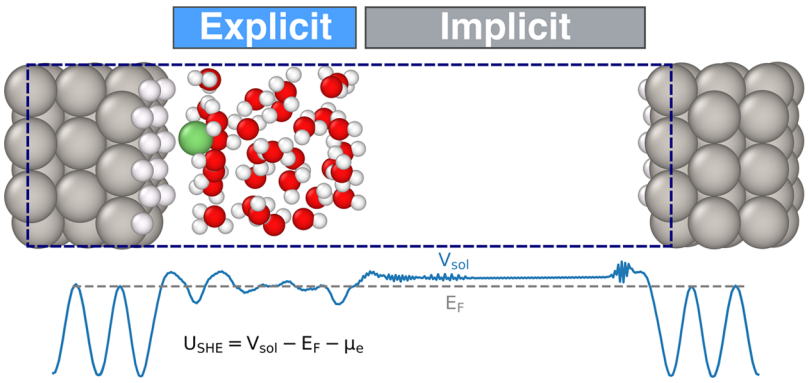

Figure 1. Supercell of 1 ML H_{upd} covered Pt(111) with explicit and implicit water regions employed in this study to identify reaction intermediates of Pt cathodic corrosion. The slab with explicit solution was used to model Pt dissolution. The implicit solvent region was added to simulate the bulk water in the postprocessing to estimate the electrode potential (U_{SHE}) via the hybrid scheme.[40−42]

the use of surfactants or capping agents.[23,29,31] One may also envision that corrosion intermediates could be exploited as highly reactive reducing species for a variety of electrocatalytical reactions.[32] Yet, to achieve desirable outcomes going beyond trial-and-error experimentation, a fundamental understanding of the cathodic corrosion process is warranted. Given the challenges associated with experimental characterizations of cathodically corroding interfaces, the application of DFT approaches can bring valuable atomistic insights.

The standard theoretical framework to analyze reactions at electrochemical interfaces does not involve explicit consideration of applied bias potential. For example, the common approach in first-principles computational electrochemistry[33,34] is to compute the total energy of the system assuming the values of U_{SHE} = 0 V and pH = 0 for the electrode potential and solution pH, respectively, and then introduce *a posteriori* corrections as

$$\Delta G(U_{SHE}, a_{H^+}) = \Delta G_0 + eU_{SHE} - k_B T \ln a_{H^+}$$

where ΔG_0 is the total energy of the system at U = 0 V and pH = 0, k_B is the Boltzmann constant, T is the temperature, and a_{H^+} is the activity of the protons. However, the electronic-structure properties of interfacial species depend on applied bias potential as it determines the amount of excess charge at the interface. Also, the overall structure of the electrical double layer and solvation of reaction intermediates at the interface are functions of electrode potential.[34−38] An ideal approach would be to perform constant-potential calculations similar to experimental conditions. Despite several proposed computational schemes,[35,39−41] at present there is no universally accepted grand-canonical theoretical framework for controlling the electrode potential in first-principles simulations.

All simulations in this work are performed within the VASP code[43,44] using the revised Perdew−Burke−Erznzerhof (RPBE) exchange-correlation functional[45,46] in conjunction with PAW potentials (Pt, O, H, Li_sv). The D3 approach within the Grimme's formalism is used to correct for nonlocal van der Waals interactions.[47,48] AIMD simulations are carried out at the Γ point of the Brillouin zone using a 1.0 fs time step and the hydrogen mass of 3 amu. The temperature is kept around 300 K using the Nose−Hoover thermostat. A plane-wave cutoff energy of 400 eV along with a smearing width of 0.1 eV within the first-order Methfessel−Paxton scheme are employed. The Pt(111)/water interface is modeled by considering a slab with 3 Pt layers and 8.32 × 9.6 Å^2 surface cell as shown in Figure 1. To simulate Pt dissolution under constant-potential conditions, we employ the constant Fermi-level AIMD approach[35,38] in combination with the blue moon ensemble method.[49,50] To evaluate an electrode potential, we use the hybrid scheme according to which an implicit water region is added to the explicitly treated water layer.[40−42] We note that other frameworks to evaluate the electrode potential from first-principles simulations were proposed, such as, for example, an intrinsic referencing scheme.[35] However, it remains unclear what computational scheme should be preferred. Since the main goal of the present study is to identify the nature of the corrosion intermediates under low cathodic potentials and how their reactivity changes with the potential, we believe that the use of the hybrid scheme is justified. All further computational details are presented in the Supporting Information.

Here, we focus on the Pt(111) surface as a model system to identify Pt corrosion intermediates under cathodic polarization. It was previously proposed in experimental literature[24,30] that alkali cations may play a key role in cathodic corrosion process by stabilizing metastable corrosion intermediates at the interface. Therefore, we consider here the atomistic models involving one and four Li ions embedded in water substituting one and four underpotential deposited hydrogen (H_{upd}) species, respectively. This is because it is known from prior computational studies that Li cations would compete with H_{upd} on Pt under low potentials.[51,52] Here, we pick the system with four Li cations as a model in which each cation has the first solvation shell of water molecules at the interface to represent a high concentration of alkali species at the interface.[53]

Figure 2 shows the time evolution of the system charge (Q) and instantaneous Fermi level (E_F) in constant Fermi-level AIMD during pre-equilibration stage for the exemplary case of the perfect Pt(111) facet with one solvated Li ion. The trajectory is split into two regions corresponding to constant-charge (5 ps) and subsequent constant-potential (2 ps) simulations. ΔQ in Figure 2 is defined as the difference between the total number of electrons in the system with extra charge (Q) and the one with no added electrons ($Q_{neutral}$) normalized per the total number of Pt atoms in the slab (n_{Pt}). It can be seen that the deviation of the Fermi level values from the average is quite substantial in the constant-charge region, whereas it is under control within the preset interval of ±0.05 eV ($\Delta\epsilon$) in the constant-potential region.

https://doi.org/10.1021/acs.jpclett.1c04187
J. Phys. Chem. Lett. 2022, 13, 3047−3052

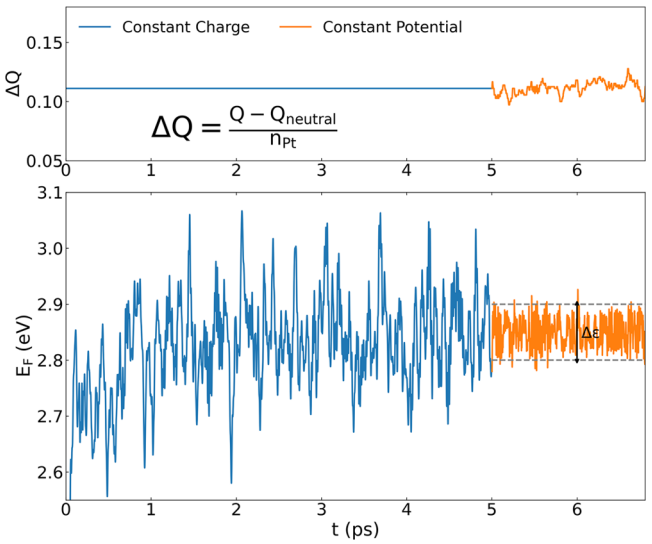

Figure 2. Time evolution of the total electronic charge Q relative to the charge of the neutral system $Q_{neutral}$ given per number of Pt atoms n_{Pt} (upper panel) and instantaneous Fermi level E_F (bottom panel) during constant-charge (first 5 ps, blue lines) and constant-potential (next 2 ps, orange lines) calculations. During constant Fermi-level AIMD simulations, E_F was allowed to vary within the preset range of $\Delta\epsilon$ = 0.1 eV.

After the systems are pre-equilibrated, we commence the constant-potential AIMD simulations of Pt dissolution from the surface using the thermodynamic integration approach. This method allows us to monitor the evolution of Pt dissolution intermediates along each dissolution trajectory. Figure 3 shows the forces and energies along two dissolution profiles: (a) with one Li and (b) with four Li cations at the surface. It can be seen from the figures that the energy reaches a plato in both cases at around 3 Å distance between the dissolved Pt species and the surface. This corresponds to a sizable drop in atomic forces that is significantly higher for the four Li case, indicating a more substantial stabilization of the Pt corrosion intermediate in a highly concentrated electrolyte.

Atomic structures of the observed dissolution intermediates are shown in Figure 4. First, it is seen that under such low cathodic potentials Li cations are partially desolvated and specifically adsorbed on the Pt surface. Upon Pt dissolution into the electrolyte, Li cations remain in the first coordination shell of the dissolving Pt species. The composition of the identified corrosion intermediate in state 1Li@Pt_{diss} for the case of one Li cation at the interface is $LiPtH_2$ (see Figure 4b). In this configuration, the interatomic distances between Li and dissolved Pt is 2.56 Å, while the Pt−H distances are 1.57 and 2.03 Å. When dissolving Pt is pushed even deeper into the electrolyte (beyond state 1Li@Pt_{diss} in Figure 3a), the dissolution barrier increases further. This process is associated with destabilization of the Pt hydride as it looses its coordination with the surrounding Li ions. In the case of the four Li system, PtH_2 in state 4Li@Pt_{diss} (Figure 4) is bonded to three Li cations at the interface with an average Pt−Li distance of 2.90 Å, while the average Pt−H bond length is 1.98 Å.

Table 1 lists the computed Bader charges on atoms at both the pristine surface and the one with dissolved Pt corresponding to the atomic structures shown in Figure 4. The charges are presented for both the one and four Li systems

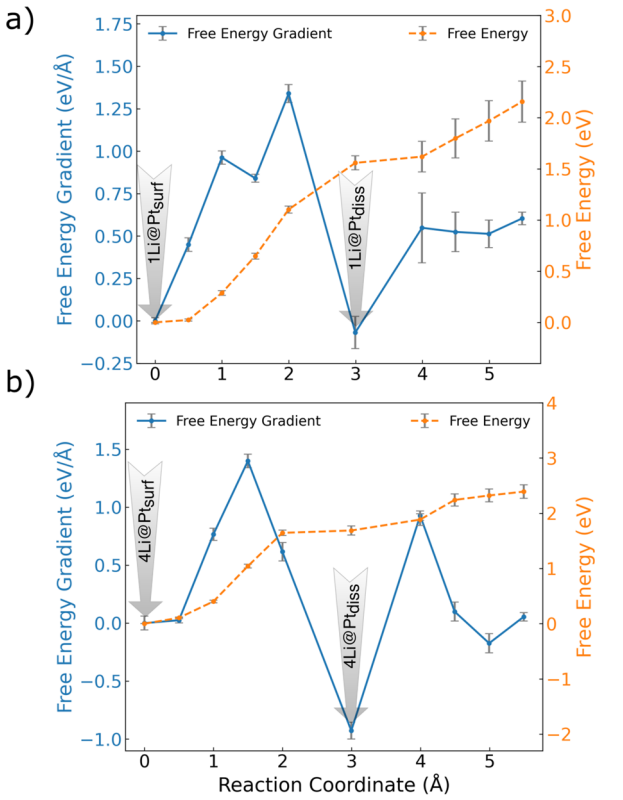

Figure 3. Free-energy profiles for Pt dissolution into the electrolyte with one (a) and four (b) Li species at the interface computed using constant-potential thermodynamic integration AIMD simulations. The estimated electrode potentials are U_{SHE} = −2.49 V (a) and U_{SHE} = −2.68 V (b). Both initial (at 0 Å) and final (at 3 Å) Pt dissolution states are depicted by arrows, while the corresponding atomic structures are presented in Figure 4.

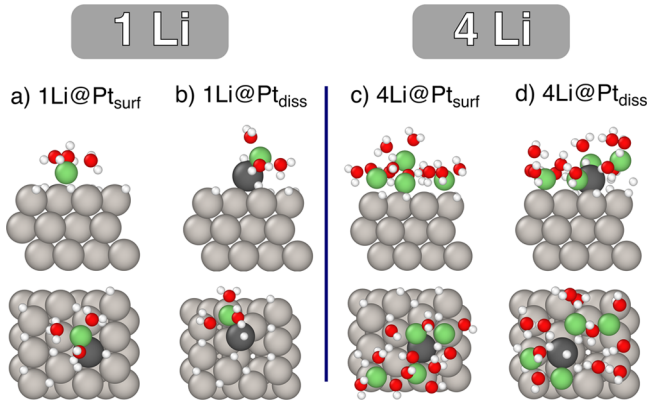

Figure 4. Side and top views of the optimized surface structures with the dissolving Pt species corresponding to different AIMD snapshots from the dissolution pathways shown in Figure 3 with one and four Li cations at the interface. The color coding is as follows: dissolving Pt - dark gray, slab Pt - light gray, Li - green, O - red, and H - white.

as a function of electrode potential. First of all, the analysis reveals negative oxidation states of both Pt and H atoms in the dissolved PtH_x species, while Li cations retain their positive charge of about 0.9 across all the cases. Moreover, it is seen that both Pt and H species are gaining more negative charge when the applied bias potential becomes more cathodic. This effect is especially pronounced for the dissolved Pt hydrides that accumulate more negative charge than the surface Pt

https://doi.org/10.1021/acs.jpclett.1c04187
J. Phys. Chem. Lett. 2022, 13, 3047−3052

Table 1. Bader Atomic Charges for Different Pt Dissolution States Shown in Figure 4 as a Function of Electrode Potential U_{SHE}[a]

	Pt	H_{Pt}	H_{surf}	Pt	H_{Pt}	H_{surf}	Pt	H_{Pt}	H_{surf}
	U = −0.30 V			U = −1.11 V			U = −1.33 V		
1Li@Pt_{surf}	−0.07		−0.08	−0.12		−0.09	−0.14		−0.1
1Li@Pt_{diss}	−0.15	−0.17	−0.03	−0.24	−0.2	−0.04	−0.34	−0.25	−0.05
	U = −1.07 V			U = −1.76 V			U = −2.37 V		
4Li@Pt_{surf}	−0.26		−0.08	−0.27		−0.09	−0.29		−0.08
4Li@Pt_{diss}	−0.52	−0.26	−0.04	−0.57	−0.26	−0.05	−0.67	−0.25	−0.06

[a]Pt stands for the dissolving Pt species, H_{Pt} - two H atoms belonging to dissolving Pt (the average value is provided), and H_{surf} - surface H.

atoms. On the other hand, the charge on the H_{upd} species is much less sensitive to the changes in electrode potential. We note that negative oxidation states of Pt are uncommon for the aqueous Pt chemistry, but were previously detected in certain solid state compounds.[19]

Having identified the cathodic corrosion intermediates, we next quantify their reactivity toward H_2 generation at the interface. This reaction was previously proposed as a sink of corrosion intermediates by which the negatively charged Pt species are discharged to regain their neutral oxidation state and precipitate back to the surface.[22−24] To this end, we analyze the thermodynamics of the H_2 formation catalyzed by corrosion intermediates reacting at the interface with either electrolyte H_2O or surface-bound H_{upd}:

$$Li_xPt^{(-z)}H_2 + H_2O \rightarrow Li_xPt^{(-z+1)}H + H_2 + OH^- \quad (1)$$

$$Li_xPt^{(-z)}H_2 + H_{ads} \rightarrow Li_xPt^{(-z+1)}H + H_2 \quad (2)$$

where x is the number of Li cations in the system and z is the Pt charge number.

The computed reaction free energies are plotted as a function of applied bias potential in Figure 5. Here, we analyze

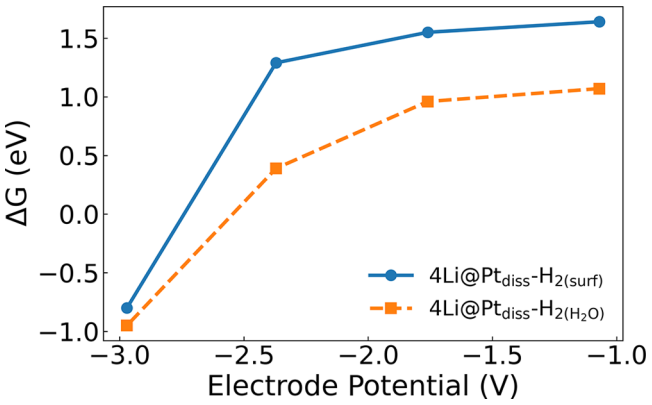

Figure 5. Free energies of the discharge reactions (1) and (2) as a function of applied bias potential for the 4Li@Pt_{diss} dissolution state shown in Figure 4d. Both initial and final atomic configurations for each reaction were optimized at a given electrode potential after being extracted from AIMD trajectories.

the corrosion intermediate in the 4Li@Pt_{diss} dissolution state (Figure 4d). It can be seen that the reaction between the Pt hydride and H_2O from the electrolyte is thermodynamically more favorable than the reaction pathway involving adsorbed hydrogen species. Also, as the electrode potential is decreased, the thermodynamic driving force to produce H_2 becomes much greater. This reactivity trend is consistent with larger negative Bader atomic charges gained by the Pt hydrides at more cathodic potentials.

In summary, we employed the constant Fermi-level molecular dynamics in conjunction with the blue moon approach to simulate Pt cathodic dissolution under the conditions of constant electrode potential. We reveal the formation of alkali cation-stabilized Pt hydrides as cathodic corrosion intermediates, thus supporting a previous hypothesis put forward in experimental literature. Our computational study thus provides the first direct evidence for the electrochemical generation of Pt anions in concentrated aqueous electrolytes similar to the previously detected negatively charged Pt species in solid state compounds. We note, however, that further investigations are warranted to achieve a complete understanding of the overall atomistic mechanism of cathodic corrosion. On the basis of the computed reaction free energies, we find that these Pt hydrides may discharge at the interface to generate H_2 by reacting with either adsorbed hydrogen species or water molecules from solution. We also determine that the corrosion intermediates become more reactive toward H_2 production under more cathodic polarizations as they are gaining more negative charge at the electrode. Overall, our computational results provide new atomic-scale insights into the interfacial electrochemistry of Pt under cathodic polarizations.

■ ASSOCIATED CONTENT

Supporting Information

The Supporting Information is available free of charge at https://pubs.acs.org/doi/10.1021/acs.jpclett.1c04187.

A detailed description of the computational methodology (PDF)

■ AUTHOR INFORMATION

Corresponding Author

Vitaly Alexandrov − *Department of Chemical and Biomolecular Engineering, University of Nebraska-Lincoln, Lincoln, Nebraska 68588, United States; Nebraska Center for Materials and Nanoscience, University of Nebraska-Lincoln, Lincoln, Nebraska 68588, United States;* orcid.org/0000-0003-2063-6914; Phone: +1 (402) 472-5323; Email: valexandrov2@unl.edu; Fax: +1 (402) 472-5323

Authors

Iman Evazzade − *Department of Chemical and Biomolecular Engineering, University of Nebraska-Lincoln, Lincoln, Nebraska 68588, United States*

https://doi.org/10.1021/acs.jpclett.1c04187
J. Phys. Chem. Lett. 2022, 13, 3047−3052

Alexandra Zagalskaya − *Department of Chemical and Biomolecular Engineering, University of Nebraska-Lincoln, Lincoln, Nebraska 68588, United States*

Complete contact information is available at: https://pubs.acs.org/10.1021/acs.jpclett.1c04187

Notes

The authors declare no competing financial interest.

■ ACKNOWLEDGMENTS

We acknowledge funding support from the National Science Foundation (NSF) through the NSF CAREER award (Grant No. CBET-1941204). This research used resources of the National Energy Research Scientific Computing Center, a DOE Office of Science User Facility supported by the Office of Science of the U.S. Department of Energy under Contract No. DE-AC02-05CH11231, as well as the Holland Computing Center at the University of Nebraska-Lincoln.

■ REFERENCES

(1) Gehlen, A. N.; D'une Letter de, M.; Gehlen, a M. Descostils, sur Plusieurs Experiences Galvaniques. *Ann. Chim.* **1808**, *66*, 191−193.
(2) Davy, H. The Bakerian Lecture for 1809. On Some New Electrochemical Researches, on Various Objects, Particularly the Metallic Bodies, from the Alkalies, and Earths, and on Some Combinations of Hydrogene. *Philos. Trans. R. Soc. London* **1810**, *100*, 16−74.
(3) Davy, H. On the Corrosion of Copper Sheeting by Sea Water, and on Methods of Preventing This Effect; and on Their Application to Ships of War and Other Ships. *Philos. Trans. R. Soc. London* **1824**, *114*, 151−158.
(4) Reed, C. J. A. Remarkable Electrolytic Phenomenon. *J. Franklin Inst.* **1895**, *139*, 283−286.
(5) Haber, F. The Phenomenon of the Formation of Metallic Dust from Cathodes. *Trans. Am. Electrochem. Soc.* **1902**, *2*, 189−196.
(6) Damjanovic, A.; Dey, A.; Bockris, J. Kinetics of Oxygen Evolution and Dissolution on Platinum Electrodes. *Electrochim. Acta* **1966**, *11*, 791−814.
(7) Frankel, G. S. Pitting Corrosion of Metals: A Review of the Critical Factors. *J. Electrochem. Soc.* **1998**, *145*, 2186.
(8) Bard, A. J., Stratmann, M., Frankel, G. S., Eds. *Encyclopedia of Electrochemistry: Corrosion and Oxide Films*; Wiley-VCH Verlag GmbH, 2003.
(9) Cherevko, S.; Reier, T.; Zeradjanin, A. R.; Pawolek, Z.; Strasser, P.; Mayrhofer, K. J. Stability of nanostructured iridium oxide electrocatalysts during oxygen evolution reaction in acidic environment. *Electrochem. Commun.* **2014**, *48*, 81−85.
(10) Reier, T.; Pawolek, Z.; Cherevko, S.; Bruns, M.; Jones, T.; Teschner, D.; Selve, S.; Bergmann, A.; Nong, H. N.; Schlögl, R.; Mayrhofer, K. J. J.; Strasser, P. Molecular Insight in Structure and Activity of Highly Efficient, Low-Ir Ir−Ni Oxide Catalysts for Electrochemical Water Splitting (OER). *J. Am. Chem. Soc.* **2015**, *137*, 13031−13040.
(11) Cherevko, S.; Geiger, S.; Kasian, O.; Kulyk, N.; Grote, J.-P.; Savan, A.; Shrestha, B. R.; Merzlikin, S.; Breitbach, B.; Ludwig, A.; Mayrhofer, K. J. Oxygen and Hydrogen Evolution Reactions on Ru, RuO_2, Ir, and IrO_2 Thin Film Electrodes in Acidic and Alkaline Electrolytes: A Comparative Study on Activity and Stability. *Catal. Today* **2016**, *262*, 170−180.
(12) Cherevko, S. Stability and Dissolution of Electrocatalysts: Building the Bridge between Model and "Real World" Systems. *Current Opinion in Electrochemistry* **2018**, *8*, 118−125.
(13) Klyukin, K.; Zagalskaya, A.; Alexandrov, V. Role of Dissolution Intermediates in Promoting Oxygen Evolution Reaction at RuO_2(110) Surface. *J. Phys. Chem. C* **2019**, *123*, 22151−22157.
(14) Zagalskaya, A.; Alexandrov, V. Mechanistic Study of IrO_2 Dissolution during the Electrocatalytic Oxygen Evolution Reaction. *J. Phys. Chem. Lett.* **2020**, *11*, 2695−2700.
(15) Escalera-López, D.; Czioska, S.; Geppert, J.; Boubnov, A.; Röse, P.; Saraçi, E.; Krewer, U.; Grunwaldt, J.-D.; Cherevko, S. Phase- and Surface Composition-Dependent Electrochemical Stability of Ir-Ru Nanoparticles during Oxygen Evolution Reaction. *ACS Catal.* **2021**, *11*, 9300−9316.
(16) Over, H. Fundamental Studies of Planar Single-Crystalline Oxide Model Electrodes (RuO_2, IrO_2) for Acidic Water Splitting. *ACS Catal.* **2021**, *11*, 8848−8871.
(17) Karpov, A.; Nuss, J.; Wedig, U.; Jansen, M. Cs_2Pt: A Platinide(-II) Exhibiting Complete Charge Separation. *Angew. Chem., Int. Ed.* **2003**, *42*, 4818−4821.
(18) Karpov, A.; Nuss, J.; Wedig, U.; Jansen, M. Covalently Bonded $[Pt]^-$ Chains in BaPt: Extension of the Zintl-Klemm Concept to Anionic Transition Metals? *J. Am. Chem. Soc.* **2004**, *126*, 14123−14128.
(19) Karpov, A.; Konuma, M.; Jansen, M. An Experimental Proof for Negative Oxidation States of Platinum: ESCA-Measurements on Barium Platinides. *Chem. Commun.* **2006**, 838−840.
(20) Fässler, T. F., Ed. *Zintl Phases: Principles and Recent Developments*; Springer-Verlag: Berlin, 2011.
(21) Kauzlarich, S. M.; Zevalkink, A.; Toberer, E.; Snyder, G. J. *Thermoelectric Materials and Devices*; The Royal Society of Chemistry, 2017; pp 1−26.
(22) Yanson, Y. I.; Yanson, A. I. Cathodic Corrosion. I. Mechanism of Corrosion via Formation of Metal Anions in Aqueous Medium. *Low Temperature Physics* **2013**, *39*, 304−311.
(23) Yanson, A. I.; Yanson, Y. I. Cathodic Corrosion. II. Properties of Nanoparticles Synthesized by Cathodic Corrosion. *Low Temperature Physics* **2013**, *39*, 312−317.
(24) Hersbach, T. J.; Koper, M. T. Cathodic Corrosion: 21st Century Insights into a 19th Century Phenomenon. *Current Opinion in Electrochemistry* **2021**, *26*, 100653.
(25) Arulmozhi, N.; Hersbach, T. J. P.; Koper, M. T. M. Nanoscale Morphological Evolution of Monocrystalline Pt Surfaces during Cathodic Corrosion. *Proc. Natl. Acad. Sci. U. S. A.* **2020**, *117*, 32267−32277.
(26) Noël, J.-M.; Yu, Y.; Mirkin, M. V. Dissolution of Pt at Moderately Negative Potentials during Oxygen Reduction in Water and Organic Media. *Langmuir* **2013**, *29*, 1346−1350.
(27) Bae, J. H.; Brocenschi, R. F.; Kisslinger, K.; Xin, H. L.; Mirkin, M. V. Dissolution of Pt during Oxygen Reduction Reaction Produces Pt Nanoparticles. *Anal. Chem.* **2017**, *89*, 12618−12621.
(28) Percival, S. J.; Dick, J. E.; Bard, A. J. Cathodically Dissolved Platinum Resulting from the O_2 and H_2O_2 Reduction Reactions on Platinum Ultramicroelectrodes. *Anal. Chem.* **2017**, *89*, 3087−3092.
(29) Yanson, A. I.; Rodriguez, P.; Garcia-Araez, N.; Mom, R. V.; Tichelaar, F. D.; Koper, M. T. M. Cathodic Corrosion: A Quick, Clean, and Versatile Method for the Synthesis of Metallic Nanoparticles. *Angew. Chem., Int. Ed.* **2011**, *50*, 6346−6350.
(30) Hersbach, T. J. P.; McCrum, I. T.; Anastasiadou, D.; Wever, R.; Calle-Vallejo, F.; Koper, M. T. M. Alkali Metal Cation Effects in Structuring Pt, Rh, and Au Surfaces through Cathodic Corrosion. *ACS Appl. Mater. Interfaces* **2018**, *10*, 39363−39379.
(31) Wirtanen, T.; Prenzel, T.; Tessonnier, J.-P.; Waldvogel, S. R. Cathodic Corrosion of Metal Electrodes—How to Prevent It in Electroorganic Synthesis. *Chem. Rev.* **2021**, *121*, 10241−10270.
(32) Hersbach, T. J. P.; Ye, C.; Garcia, A. C.; Koper, M. T. M. Tailoring the Electrocatalytic Activity and Selectivity of Pt(111) through Cathodic Corrosion. *ACS Catal.* **2020**, *10*, 15104−15113.
(33) Calle-Vallejo, F.; Koper, M. T. First-Principles Computational Electrochemistry: Achievements and Challenges. *Electrochim. Acta* **2012**, *84*, 3−11.
(34) Groß, A. *Atomic-Scale Modelling of Electrochemical Systems*; John Wiley & Sons, Ltd, 2021; Chapter 6, pp 201−220.

(35) Bouzid, A.; Pasquarello, A. Atomic-Scale Simulation of Electrochemical Processes at Electrode/Water Interfaces under Referenced Bias Potential. *J. Phys. Chem. Lett.* **2018**, *9*, 1880−1884.
(36) Zhang, C.; Hutter, J.; Sprik, M. Coupling of Surface Chemistry and Electric Double Layer at TiO_2 Electrochemical Interfaces. *J. Phys. Chem. Lett.* **2019**, *10*, 3871−3876.
(37) Groß, A.; Sakong, S. Modelling the Electric Double Layer at Electrode/Electrolyte Interfaces. *Current Opinion in Electrochemistry* **2019**, *14*, 1−6.
(38) Bouzid, A.; Pasquarello, A. *Atomic-Scale Modelling of Electrochemical Systems*; John Wiley & Sons, Ltd, 2021; Chapter 7, pp 221−240.
(39) Le, J.; Iannuzzi, M.; Cuesta, A.; Cheng, J. Determining Potentials of Zero Charge of Metal Electrodes versus the Standard Hydrogen Electrode from Density-Functional-Theory-Based Molecular Dynamics. *Phys. Rev. Lett.* **2017**, *119*, 016801.
(40) Cheng, T.; Wang, L.; Merinov, B. V.; Goddard, W. A. Explanation of Dramatic pH-Dependence of Hydrogen Binding on Noble Metal Electrode: Greatly Weakened Water Adsorption at High pH. *J. Am. Chem. Soc.* **2018**, *140*, 7787−7790.
(41) Zhao, X.; Liu, Y. Origin of Selective Production of Hydrogen Peroxide by Electrochemical Oxygen Reduction. *J. Am. Chem. Soc.* **2021**, *143*, 9423−9428.
(42) Zagalskaya, A.; Evazzade, I.; Alexandrov, V. Ab Initio Thermodynamics and Kinetics of the Lattice Oxygen Evolution Reaction in Iridium Oxides. *ACS Energy Letters* **2021**, *6*, 1124−1133.
(43) Kresse, G.; Furthmüller, J. Efficient Iterative Schemes for Ab Initio Total-Energy Calculations Using a Plane-Wave Basis Set. *Phys. Rev. B* **1996**, *54*, 11169−11186.
(44) Kresse, G.; Furthmuller, J. Efficiency of Ab-Initio Total Energy Calculations for Metals and Semiconductors Using a Plane-Wave Basis Set. *Comput. Mater. Sci.* **1996**, *6*, 15−50.
(45) Perdew, J. P.; Burke, K.; Ernzerhof, M. Generalized Gradient Approximation Made Simple. *Phys. Rev. Lett.* **1996**, *77*, 3865.
(46) Zhang, Y.; Yang, W. Comment on "Generalized Gradient Approximation Made Simple. *Phys. Rev. Lett.* **1998**, *80*, 890.
(47) Grimme, S.; Antony, J.; Ehrlich, S.; Krieg, H. A Consistent and Accurate Ab Initio Parametrization of Density Functional Dispersion Correction (DFT-D) for the 94 Elements H-Pu. *J. Chem. Phys.* **2010**, *132*.154104
(48) Grimme, S.; Ehrlich, S.; Goerigk, L. Effect of the Damping Function in Dispersion Corrected Density Functional Theory. *J. Comput. Chem.* **2011**, *32*, 1456−1465.
(49) Carter, E.; Ciccotti, G.; Hynes, J. T.; Kapral, R. Constrained Reaction Coordinate Dynamics for the Simulation of Rare Events. *Chem. Phys. Lett.* **1989**, *156*, 472−477.
(50) Sprik, M.; Ciccotti, G. Free Energy from Constrained Molecular Dynamics. *J. Chem. Phys.* **1998**, *109*, 7737−7744.
(51) Mills, J. N.; McCrum, I. T.; Janik, M. J. Alkali Cation Specific Adsorption onto fcc(111) Transition Metal Electrodes. *Phys. Chem. Chem. Phys.* **2014**, *16*, 13699−13707.
(52) McCrum, I. T.; Janik, M. J. pH and Alkali Cation Effects on the Pt Cyclic Voltammogram Explained Using Density Functional Theory. *J. Phys. Chem. C* **2016**, *120*, 457−471.
(53) Garlyyev, B.; Xue, S.; Watzele, S.; Scieszka, D.; Bandarenka, A. S. Influence of the Nature of the Alkali Metal Cations on the Electrical Double-Layer Capacitance of Model Pt(111) and Au(111) Electrodes. *J. Phys. Chem. Lett.* **2018**, *9*, 1927−1930.

https://doi.org/10.1021/acs.jpclett.1c04187
J. Phys. Chem. Lett. 2022, 13, 3047−3052